Article

# Secondary Nucleation and Growth of ZnO

Thomas L. Sounart, Jun Liu, James A. Voigt, Mae Huo, Erik D. Spoerke, and Bonnie McKenzie

*J. Am. Chem. Soc.*, **2007**, 129 (51), 15786-15793 • DOI: 10.1021/ja071209g



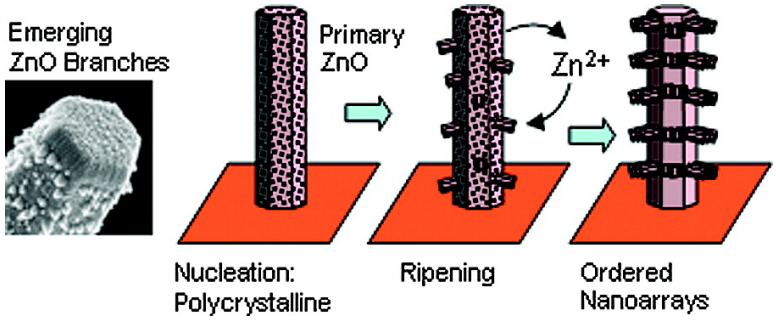

J|A|C|S
ARTICLES
Published on Web 11/29/2007

# Secondary Nucleation and Growth of ZnO

Thomas L. Sounart,*,† Jun Liu,‡ James A. Voigt, Mae Huo, Erik D. Spoerke, and Bonnie McKenzie

*Contribution from Sandia National Laboratories, P.O. Box 5800, Albuquerque, New Mexico 87185*

Received February 19, 2007; E-mail: thomas.l.sounart@intel.com

***Abstract:*** Recently we discovered that under certain conditions new crystal growth (branch) can be induced on specific crystalline planes of the same material. This is a new phenomenon and is in sharp contrast to typical nucleation and growth in which a crystal will simply grow larger in preferred directions depending on the surface energy of the specific crystalline planes. Based on our observation, we developed a sequential nucleation and growth technique offering the power to assemble complex hierarchical crystals step-by-step. However, the key questions of when and how the secondary nucleation takes place have not been answered. Here we systematically study secondary ZnO crystal growth using organic diamine additives with a range of chain lengths and concentration. We found that ZnO branches form for a narrow diamine concentration range with a critical lower and upper critical nucleation concentration limit, which increases by about a factor of 5 for each additional carbon in the diaminoalkane chain. Our results suggest that the narrow window for secondary growth is dictated by the solubility of the ZnO crystals, where the low critical nucleation concentration is determined by slight etching of the surface to produce new nucleation sites, and the upper critical concentration is determined by the supersaturation concentration. Kinetic measurements show that the induction time and growth rate increase with increasing diamine concentration and follow classical nucleation and growth theory. Observations of branch morphological evolution reveal the mechanisms guiding the tunable crystal size and morphology.

## Introduction

Nanostructured inorganic crystals with tunable morphology are desirable for optimization in many potential applications in energy conversion, electronics, catalysis, optics, chemical sensing, and medicine. Controlled growth of hierarchical crystal architectures has received particular attention recently[1,2] to support application demands for more complex structures to impart greater control over material and device properties. Although fabrication of structures with the complexity observed in natural materials or biominerals[3] remains a significant challenge, substantial progress has been made in the control of branched hierarchical crystals. Gas-phase synthesis techniques have been used to grow branched nanocrystals for several material systems,[4−15] and many types of branched nanocrystals have also been produced with solution-phase synthesis,[16−35] which offers the potential for low-cost, industrial-scale manufacturing.

The most common branched nanocrystals formed in solution are mulitipod,[18−23,28,29,34,35] star-shaped,[32] and nanoflower or nanothorn structures,[31,33] in which branches grow outward from a central nucleus in a single reaction stage. The underlying mechanism offered for many of these are either anisotropic

† Current Address: Intel Corporation, 4500 Dobson Rd, Chandler, AZ 85248.

‡ Current Address: Pacific Northwest National Laboratories, 902 Battelle Boulevard, K2-50, Box 999, Richland, WA 99352.

(1) Sounart, T. L.; Liu, J.; Voigt, J. A.; Hsu, J.; Spoerke, E. D.; Tian, Z.; Jiang, Y. *Adv. Funct. Mater.* **2006**, *16*, 335−344.
(2) Tian, Z. R.; Liu, J.; Voigt, J. A.; Mckenzie, B.; Huifang, X. *Angew. Chem., Int. Ed.* **2003**, *42*, 413−417.
(3) Jackson, A.; Vincent, J.; Turner, R. *Proc. R. Soc. London, Ser. B* **1988**, *234*, 415−440.
(4) Dick, K. A.; Deppert, K.; Larsson, M.; Martensson, T.; Seifert, W.; Wallenberg, L.; Samuelson, L. *Nat. Mater.* **2004**, *3*, 380−384.
(5) Dick, K. A.; Geretovszky, Z.; Mikkelsen, A.; Karlsson, L. S.; Lundgren, E.; Malm, J.-O.; Andersen, J. N.; Samuelson, L.; Seifert, W.; Wacaser, B. A.; Deppert, K. *Nanotechnology* **2006**, *17*, 1344−1350.
(6) Fonseca, L. F.; Resto, O.; Sola', F. *Appl. Phys. Lett.* **2005**, *87*, 113111.
(7) Gao, X. P.; Wang, Z. L. *Appl. Phys. Lett.* **2004**, *84*, 2883−2885.
(8) Gao, P. X.; Wang, Z. L. *J. Phys. Chem. B* **2002**, *106*, 12653−12658.
(9) Huang, Y. H.; Zhang, Y.; Bai, X. D.; He, J.; Liu, J.; Zhang, X. M. *J. Nanosci. Nanotechnol.* **2006**, *6*, 2566−2570.
(10) Lao, J. Y.; Wen, J. G.; Ren, Z. F. *Nano Lett.* **2002**, *2*, 1287−1291.
(11) Shen, G.; Bando, Y.; Lee, C.-J. *J. Phys. Chem. B* **2005**, *109*, 10779−10785.
(12) Shen, G. Z.; Lee, C. J. *Cryst. Growth Des.* **2005**, *5*, 1085−1089.
(13) Wan, Q.; Wei, M.; Zhi, D.; MacManus-Driscoll, J. L.; Blamire, M. G. *Adv. Mater.* **2006**, *18*, 234−235.
(14) Wei, D.; Liu, Y.; Cao, L.; Fu, L.; Li, X.; Wang, Y.; Yu, G.; Zhu, D. *Nano Lett.* **2006**, *6*, 186−192.
(15) Ying, Z.; Wan, Q.; Song, Z. T.; Feng, S. L. *Mater. Lett.* **2005**, *59*, 1670−1672.
(16) Cheng, W.; Wang, W.; Chen, D.; Bao, F. *J. Phys. Chem. B* **2005**, *109*, 794−798.
(17) Ding, Y. S.; Shen, X. F.; Gomez, S.; Luo, H.; Aindow, M.; Suib, S. L. *Adv. Funct. Mater.* **2006**, *16*, 549−555.
(18) Grebinski, J. W.; Hull, K. L.; Zhang, J.; Kosel, T. H.; Kuno, M. *Chem. Mater.* **2004**, *16*, 5260−5272.
(19) Hull, K. L.; Grebinski, J. W.; Kosel, T. H.; Kuno, M. *Chem. Mater.* **2005**, *17*, 4416−4425.
(20) Jun, Y. W.; Jung, Y. Y.; Cheon, J. *J. Am. Chem. Soc.* **2002**, *124*, 615−619.
(21) Jun, Y. W.; Lee, S. M.; Kang, N. J.; Cheon, J. *J. Am. Chem. Soc.* **2001**, *123*, 5150−5151.
(22) Manna, L.; Milliron, D. J.; Meisel, A.; Scher, E. C.; Alivisatos, A. P. *Nat. Mater.* **2003**, *2*, 382−385.
(23) Manna, L.; Scher, E. C.; Alivisatos, A. P. *J. Am. Chem. Soc.* **2000**, *122*, 12700−12706.
(24) Meng, G. W.; Jung, Y. J.; Cao, A. Y.; Vajtai, R.; Ajayan, P. M. *Proc. Natl. Acad. Sci. U.S.A.* **2005**, *102*, 7074−7078.


**10.1021/ja071209g CCC: $37.00** 

growth in preferred directions from a twinned nucleus or polymorphic growth through stacking faults on the fastest-growing facets of the nucleus.[18,20,23,32,34] Hyperbranched crystals with numerous branches might grow from a core of multiple nuclei, and other mechanisms might be inciting further nucleation on existing branched crystals,[33,35] a phenomenon that is not well-understood. Dendritic nanocrystals have also been observed[16,25,30] and are often explained by a mechanism of oriented attachment[16] but may also be created by renucleation events.[30,35]

Several groups have recently used multiple synthesis steps to nucleate new oriented nanocrystals on crystals formed in a previous reaction step. This provides the capability to build a diverse range of complex nanostructures from various primary subunits that can be tuned by the growth chemistry in each step. In gas-phase synthesis, Dick et al.[4,5] first synthesized GaP and InAs semiconductor nanowires and then sequentially reseeded the nanowire surfaces to produce treelike nanostructures. In solution-phase synthesis, the multistep approach has been used primarily to synthesize branched heterostuctures, including PbSe nanocrystals on the tips of CdS/CdSe nanorods,[36] $SnO_2$ branches on $\alpha$-$Fe_2O_3$ nanotubes,[37] $V_2O_5$ nanorods on $V_2O_5/TiO_2$ nanofibers,[38] ZnO branches on carbon nanotubes,[39] CdS nanorods on ZnO microcrystals,[1] and various $ZnO/TiO_2$-based[40] composite nanostructures. To produce these composite branched structures, material choices and solution conditions are adjusted to promote heterogeneous over homogeneous nucleation of the supersaturated branch crystal material on the primary crystal. This is similar to controlling heterogeneous nucleation and growth of nanorod arrays on a bulk substrate.[41−43]

Solution-phase synthesis of ordered ZnO branch crystals was first demonstrated by Gao et al.[44] using multistep precipitation of powders in bulk aqueous solutions under hydrothermal conditions; branch growth on the homogeneous precipitate was observed in a second stage with 5 M NaOH (pH ~13). ZnO is a material of considerable interest because it is piezoelectric, transparent, and a wide band gap semiconductor ($E_g$ = 3.37 eV) with a low exciton binding energy (60 eV). In a series of papers, we systematically demonstrated how sequential, step-by-step processes, coupled with controlled nucleation and growth and organic surface modification molecules (citrate and diamines), can be used to prepare highly oriented, complex hierarchical ZnO nanostructures on substrates.[1,45−47] In particular, recently we reported the preparation of high-order ZnO nanostructures in a controlled fashion by artificially inducing secondary and tertiary nucleation events on oriented ZnO arrays using several organic diamine molecules.[1] Very similar methods and results were discussed in a later paper by Zhang et al.,[48] which called the secondary nucleation phenomenon "site-specific nucleation" or "nanografting."

In multistage synthesis of branched ZnO crystals, oriented arrays of rod or needle-shaped crystals grow on the $\{10\bar{1}0\}$ planes of ZnO rods grown in the previous growth stages. This produces a secondary morphology that is star-shaped in an image plane orthogonal to the primary crystal *c*-axis and comblike in an image plane parallel to the primary *c*-axis. This branching morphology has also been observed for secondary ZnO crystals produced with high-temperature, vapor-phase synthesis[7,10] and in solution-phase synthesis of other material systems.[26,37] These are fundamentally different from multipod-type branched structures that grow in a single reaction stage from a central nucleus, but there are similarities in mechanism and structure such as the twin alignment of the branches[34] and, as we will show, the control of growth rate to tune the morphology.[34,35]

The key to the sequential nucleation and growth process is the ability to induce secondary nucleation of new, oriented branched crystals on primary ZnO. This is a very unusual, important phenomenon that does not occur in typical crystal growth but is not limited to ZnO.[49] In typical growth, different crystalline planes in a given crystal have different atomic densities, and atoms on different facets have a different number of unsatisfied bonds, leading to different surface energies for different facets. During crystal growth, crystals will epitaxially grow larger.[49−51] Facets with a fast growth rate tend to disappear; i.e., surfaces with high surface energy will disappear. On a thermodynamically equilibrated crystal, those surfaces with the lowest total surface energy will survive, as determined by the Wulff plot.[52,53] However, such a nucleation and growth theory cannot explain the secondary nucleation phenomena. The objective of this paper is to provide answers to several unsolved fundamental questions regarding the sequential nucleation and growth process, including where and how the secondary nucleation occurs, the critical conditions required to induce the renucleation, the role of the diamine molecules, the factors that

(25) Wang, Q. Q.; Xu, G.; Han, G. R. *Cryst. Growth Des.* **2006**, *6*, 1776−1780.
(26) Yang, W.-H.; Lee, C.-F.; Tang, H. Y.; Shieh, D.-B.; Yeh, C.-S. *J. Phys. Chem. B* **2006**, *110*, 14087−14091.
(27) Yu, S.; Wang, C.; Yu, J.; Shi, W.; Deng, R.; Zhang, H. *Nanotechnology* **2006**, *17*, 3607−3612.
(28) Zheng, D. S.; Yin, Z. L.; Zhang, W. M.; Tan, X. J.; Sun, S. X. *Cryst. Growth Des.* **2006**, *6*, 1733−1735.
(29) Zhu, W.; Wang, W.; Xu, H.; Zhou, L.; Zhang, L.; Shi, J. *J. Cryst. Growth* **2006**, *295*, 69−74.
(30) He, R.; Qian, X.; Yin, J.; Zhu, Z. *Chem. Phys. Lett.* **2003**, *369*, 454−458.
(31) Tian, N.; Zhi-You, Z.; Sun, S.-G.; Cui, L.; Ren, B.; Tian, Z.-Q. *Chem. Commun.* **2006**, *39*, 4090−4092.
(32) Nehl, C. L.; Hongwei, L.; Hafner, J. H. *Nano Lett.* **2006**, *6*, 683−688.
(33) Fang, Z.; Tang, K.; Shen, G.; Chen, D.; Kong, R.; Lei, S. *Mater. Lett.* **2006**, *60*, 2530−2533.
(34) Carbone, L.; Kudera, S.; Carlino, E.; Parak, W. J.; Giannini, C.; Cingolani, R.; Manna, L. *J. Am. Chem. Soc.* **2006**, *128*, 748−755.
(35) Kanaras, A. G.; Sonnichsen, C.; Liu, H.; Alivisatos, A. P. *Nano Lett.* **2005**, *5*, 2164−2167.
(36) Kudera, S.; Carbone, L.; Casula, M. F.; Cingolani, R.; Falqui, A.; Snoeck, E.; Parak, W. J.; Manna, L. *Nano Lett.* **2005**, *5*, 445−449.
(37) Zhang, D. F.; Sun, L. D.; Jia, C. J.; Yan, Z. G.; You, L. P.; Yan, C. H. *J. Am. Chem. Soc.* **2005**, *127*, 13492−13493.
(38) Ostermann, R.; Li, D.; Yin, Y.; McCann, J. T.; Xia, Y. *Nano Lett.* **2006**, *6*, 1297−1302.
(39) Zhang, W. D. *Nanotechnology* **2006**, *17*, 1036−1040.
(40) Yang, H.; Zeng, H. *J. Am. Chem. Soc.* **2005**, *127*, 270−278.
(41) Bunker, B. C.; Rieke, P. C.; Tarasevich, B. J.; Campbell, A. A.; Fryxell, G. E.; Graff, G. L.; Song, L.; Liu, J.; Virden, J. W. *Science* **1994**, *264*, 48−55.
(42) Boyle, D. S.; Govender, K.; O'Brien, P. *Chem. Commun.* **2002**, *1*, 80−81.
(43) Govender, K.; Boyle, D. S.; Kenway, P. B.; O'Brien, P. *J. Mater. Chem.* **2004**, *14*, 2575−2591.
(44) Gao, X.; Zheng, Z.; Zhu, H.; Pan, G.; Bao, J.; Wu, F.; Song, D. *Chem. Commun.* **2004**, *12*, 1428−1429.
(45) Tian, Z. R.; Voigt, J. A.; Liu, J.; Mckenzie, B.; Mcdermott, M. J.; Cygan, R. T.; Criscenti, L. J. *Nat. Mater.* **2003**, *2*, 821−826.
(46) Tian, Z. R. R. L. J.; Voigt, J. A.; Xu, H. F.; McDermott, M.; McKenzie, B. *Abstr. Pap. Am. Chem. S.* **2003**, *225*, U49.
(47) Hsu, J.; Tian, Z.; Simmons, N.; Matzke, C.; Voigt, J.; Liu, J. *Nano Lett.* **2005**, *5*, 83−86.
(48) Zhang, T.; Dong, W.; Keeter-Brewer, M.; Konar, S.; Njabon, R. N.; Tian, Z. R. *J. Am. Chem. Soc.* **2006**, *128*, 10960−10968.
(49) Hartman, P.; Perdok, W. G. *Acta Crystallogr.* **1955**, *8*, 49−52.
(50) Hartman, P. *Crystal Growth: An Introduction*; North Holland: Amsterdam, 1973.
(51) Hartman, P. *Z. Kristallogr.* **1965**, *121*, 78.
(52) Herring, C. In *Structure and Properties of Solid Surfaces*; Gomer, R., Smith, C. S., Eds.; University of Chicago: Chicago, 1953.
(53) Mullins, W. W. In *Metal surfaces: structure, energetics, and kinetics*; American Society for Metals: Metals Park, OH, 1962.

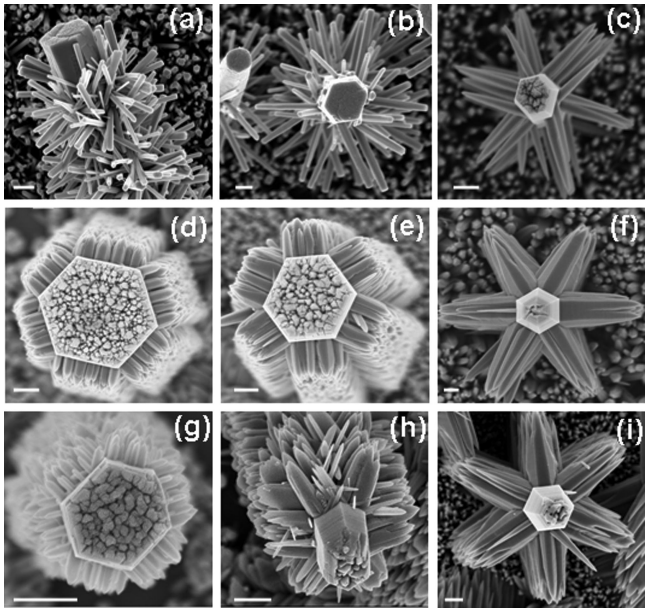


***Figure 1.*** ZnO branches for selected diamine concentrations and chain lengths (SEM images). Top row: EDA at (a) 8 mM (pH = 7.1), (b) 15 mM (pH = 7.3), (c) 40 mM (pH = 8.7). Middle row: DAP at (d) 43 mM (pH = 9.9), (e) 55 mM (pH = 10.4), (f) 80 mM (pH = 10.7). Bottom row: DAB at (g) 93 mM (pH = 11.0), (h) 266 mM (pH = 11.5), (i) 400 mM (pH = 11.7). Scale bars are 500 nm. Images of multiple crystals are provided in the Supporting Information, Figures S1 and S2, and the images are compared at the same scale in Figure S7.

control the nucleation and growth rate, and the mechanisms for forming the hierarchical structures and morphologies.

## Experimental Section

Branched ZnO crystals were synthesized using two growth stages on clean, unseeded glass substrates to produce a sparsely populated film of secondary crystalline structures. The substrates were first cleaned ultrasonically for 10 min each in methylene chloride, acetone, and water, then blown dry with $N_2$, and baked for 1 h at 450 °C. In the first growth stage, the clean glass substrates were incubated at 60 °C in 125 mL Teflon bottles containing 75 mL of aqueous solutions of 20 mM $Zn(NO_3)_2$ and 20 mM hexamethylenetetramine (HMT). This produced primary ZnO rods on nucleation sites on the glass substrate. Larger primary crystals were synthesized by adding 1.5 mg of sodium citrate to 30 mL of solution and reacted at 60 °C. After drying in air, the substrates were incubated again in a second growth stage at 60 °C in solutions of 20 mM $Zn(NO_3)_2$ and 20 mM HMT and a range of diamine concentrations and incubation times. This produced secondary nanocrystal arrays on the facets of the primary ZnO crystal. For diaminoalkane chain length comparisons, the branching stage incubation time was 8 h, and branches formed for diamine concentrations ranging from 3 to 45 mM in ethylene diamine (EDA), 30 to 130 mM diaminopropane (DAP), and 90 to 700 mM diaminobutane (DAB). For kinetic studies, DAP concentrations of 43, 80, and 130 mM were used, and incubation times ranged from 10 min to 10 h. Crystal growth on a single ZnO crystal was conducted under the same conditions using EDA.

Branch lengths were measured as the length from the primary crystal surface to the branch tip from SEM images in which the branches are oriented with their *c*-axes approximately in the image plane, e.g., the image plane normal to the primary crystal *c*-axis. The crystals do not have to be exactly in-plane to obtain a good estimate of length because the measurement is relatively insensitive to alignment. For example, for a crystal that is oriented 10° to the image plane, the error in the length measurement will be only 1.5%. For a 20° misalignment, the error is only 6%.

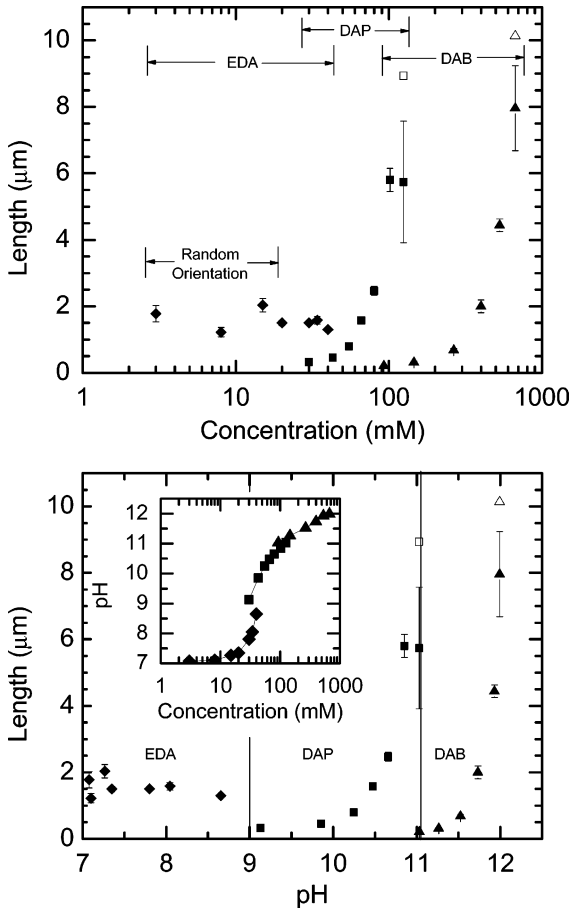


***Figure 2.*** Branch length as a function of diamine concentration, pH, and chain length. Mean: EDA, ◆; DAP, ■; DAB, ▲. Max: DAP, □; DAB, △. The lower panel shows the branch lengths plotted vs the solution pH measured for each diamine concentration (inset). The diamine concentration was the only independently controlled variable (no pH adjustments were made). The mean branch length is calculated from at least five branches sampled from at least three different crystals, and the error bars represent 1-$\sigma$ from the mean. Where error bars cannot be distinguished, $\sigma$ is less than the size of the symbol that denotes mean length.

The ZnO branches were characterized by a Zeiss field-emission source scanning electron microscope (SEM) and a JEOL 2010 FEG STEM/TEM operated at 200 kV in the Transmission Electron Microscopy Laboratory at the University of New Mexico.

## Results and Discussion

Organic diamines mediate the growth of ZnO branch crystals for a limited concentration range that varies with the hydrocarbon chain length of the diamine. Figure 1 shows secondary ZnO crystal structures (wurtzite, $a = 3.2495$ and $c = 5.2069$)[1] grown using the diamines EDA, DAP, and DAB, which have increasing hydrocarbon chain lengths from 2 to 4 carbons, respectively. For the case of EDA, the secondary branch properties, such as morphology, size, and number density, do not follow a simple trend. At low EDA concentrations, the branches are randomly oriented and polydisperse with a hexagonal rod shape (Figure 1a,b), but a discrete transition occurs at 20 mM, at which point very few branches grow (Figure S1) and above which the branches are monodisperse, aligned needles (Figure 1c). The length of the branches grown with EDA is insensitive to diamine concentration (Figure 2), whereas, for DAP and DAB, the branch growth follows a controlled, monotonic trend of increasing branch size and decreasing

number density with increasing diamine concentration, and only the aligned needle morphology is observed (Figure 1d−i, Figure 2). At the upper limit of the branching concentration range for DAP and DAB, the branches become polydisperse (cf. error bars in Figure 2) due to prolonged nucleation, but the largest crystals, which nucleate first, follow the trend.

**Critical Conditions for Branch Growth and the Role of Diaminoalkanes.** The diamine concentration range for branch growth is quite small, spanning less than or equal to about 1 order of magnitude for each of the diamines studied in this work (Figure 2). The upper bound of each growth range (45 mM for EDA, 150 mM for DAP, and 800 mM for DAB) increases by a factor of 3 to 5 for each additional carbon in the diaminoalkane chain. There are two critical diamine concentrations that bound each branch growth range: a critical nucleation concentration (CNC), below which no branches are nucleated, and an upper critical concentration, which scales with the ZnO solubility limit for each diamine. As diamine concentration is increased above the CNC, branches grow until a concentration is reached at which the level of supersaturation is too low to overcome the free energy of nucleation. Further increase leads to dissolution of the primary crystals. Thus, branch growth always occurs for diamine concentrations that regulate $Zn^{2+}$ just above saturation.

The diamine molecules control $Zn^{2+}$ solubility through two important effects on solution chemistry: (i) the amine groups of the diamines are basic and thus raise the pH, and (ii) the amine groups complex with $Zn^{2+}$, which increases zinc solubility. The pH is important because $Zn^{2+}$ and $OH^-$ form zinc−hydroxo complexes that affect zinc solubility and that precipitate as $ZnO_{(s)}$ via a dehydration reaction at elevated temperature.[54,55] If the effect on pH was the dominant mechanism controlling the zinc solubility limit (viz. if the different diamines had essentially the same effect on Zn−amino complexes but different p*K*'s), then plotting branch length vs pH would tend to collapse the growth curves in Figure 2. However, as shown in the lower panel in Figure 2, the growth curves are separated further when plotted vs the pH of the solution measured for each diamine concentration, and in fact, branch growth is observed in completely different pH regimes for each diamine (zinc saturation at pH = 9, 11, and 12 for EDA, DAP, and DAB, respectively). The inset in Figure 2 shows that the chain length has only a weak effect on the p*K* as there are only slight shifts in the titration curve from changing diamine chain length. The pH measurements show that the diamine basicity increases slightly with hydrocarbon chain length and that diamine regulation of pH is not the dominant mechanism controlling zinc solubility and thus the diamine concentration range for branch growth.

The other important effect of the diamines on the solution chemistry is complexation with $Zn^{2+}$, which reduces the concentration of free zinc, thus increasing the solubility of ZnO. The 4- to 5-fold increase in the branch-growth concentration range for each additional carbon corresponds to an increase in diamine concentration required to complex enough free zinc to approach the saturation point. The correct solubility conditions for branch growth requires about a 1 order of magnitude higher $OH^-$ concentration in addition to a factor of 3 to 5 increase in amine concentration for each added carbon in the diamine hydrocarbon chain. This suggests that the carbon chain length weakens the affinity for $Zn^{2+}$, so higher concentrations are required for longer chain lengths to complex the same amount of $Zn^{2+}$ and thereby regulate the zinc solubility to the same level.

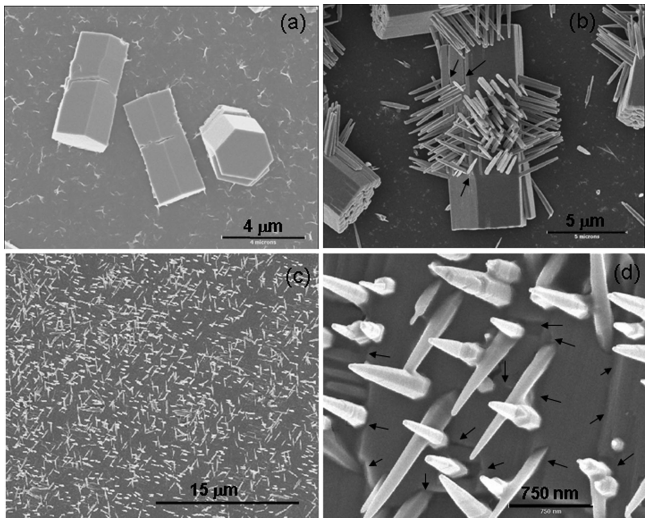


***Figure 3.*** SEM images of secondary nucleation on larger primary ZnO crystals and on $(10\bar{1}0)$ ZnO substrates. (a) Primary ZnO crystals grown with 50 mg/L citrate in the first growth stage. (b) Secondary ZnO crystal from renucleation on the primary crystals in second-stage growth. (c,d) Branch nucleation on $(10\bar{1}0)$ ZnO substrate.

**Secondary Nucleation Mechansim.** The first step in the formation of the branches is the nucleation of new crystals on the columnar facets of ZnO crystals.[1] The CNC shifts up with increasing hydrocarbon chain length similar to the shift in the upper critical concentration (saturation point), which suggests that the CNC is also driven by solubility. The CNC might be the concentration required to cause light surface dissolution (etching) of the primary ZnO crystal during the approach to the 60 °C incubation temperature, thus creating nucleation sites during supersaturation conditions at 60 °C. To understand where the renucleation takes place on the ZnO surface, we studied the nucleation of ZnO nanorods on larger primary ZnO crystals, as well as on single crystalline ZnO $(10\bar{1}0)$ prismatic surfaces. Figure 3a shows a typical hexagonal bicrystal with a joining middle plane due to the polar nature of ZnO.[1] The $\{10\bar{1}0\}$ surfaces are smooth except for the middle plane. Figure 3b shows the morphology with the growth of the branched crystals. Notice that many of the branched crystals are concentrated in the central region. Careful examination reveals a high density of line defects under the branched crystals in this central area. We believe that the line defects were created by the early dissolution event and served as pin-points for the secondary nucleation to occur. Branch growth on single crystalline ZnO (Figure 3c,d) further supports the idea that the new crystals are mostly formed on the defect sites of the $\{10\bar{1}0\}$ surfaces, such as edges and holes, as indicated by the arrows in Figure 3d. Therefore, our results support the hypothesis that the CNC may be the concentration at which light surface etching forms nucleation sites and the upper critical concentration is bound by the concentration to cause complete dissolution of the ZnO crystals.

The mechanism of branch nucleation driven by solubility is also consistent with the report of secondary nucleation of ZnO

(54) Tak, Y.; Yong, K. *J. Phys. Chem. B* **2005**, *109*, 19263−19269.
(55) Peterson, R. B.; Fields, C. L.; Gregg, B. A. *Langmuir* **2004**, *20*, 5114−5118.

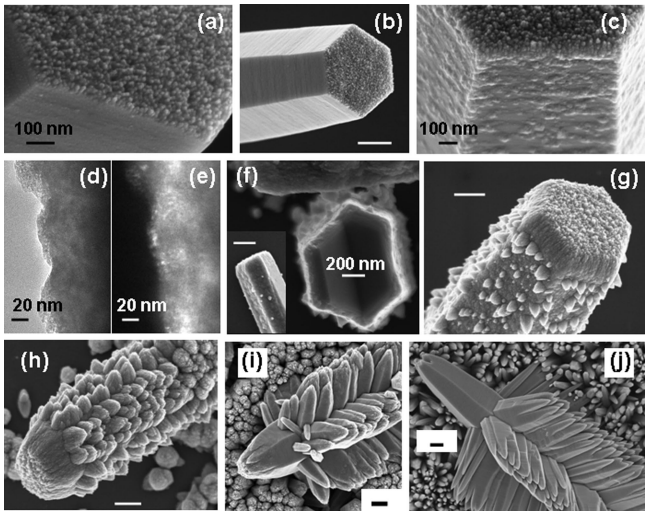


***Figure 4.*** ZnO branch crystals at selected incubation times during secondary growth stage, showing nucleation and growth kinetics for 80 mM DAP, including capture of nucleation event: (a) 10 min, (b) 20 min, (c−e) 30 min, (f) 40 min, (g) 50 min, (h) 1 h, (i) 3 h, (j) 10 h. TEM images in d (bright field) and e (dark field) show that the secondary nuclei observed in the SEM image in c are polycrystalline. All other images are from SEM. Scale bars are 500 nm except as noted. Images of multiple crystals are provided in the Supporting Information, Figure S3, and the images are compared at the same scale in Figure S8.

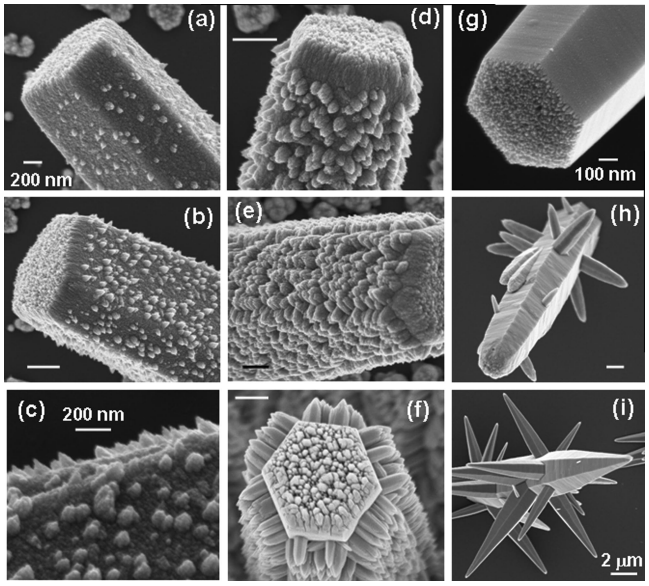


***Figure 5.*** SEM images of ZnO branch crystals at selected incubation times during secondary growth stage for (a−f) 43 mM: (a) 10, (b,c) 20, (d) 30, (e) 50, (f) 600 min; and (g−i) 125 mM: 1, 4, 10 h. Scale bars are 500 nm except as noted. Images of multiple crystals are provided in the Supporting Information, Figures S4 and S5, and the images are compared at the same scale in Figure S9.

using an entirely different chemistry, viz. NaOH solutions.[44] However, controlled tunable branch nucleation has only been demonstrated to date with diamines. The bifunctional diamine molecules might play additional roles in promoting branch nucleation. Kanaras et al.[35] observed that bifunctional phosphonic acids promoted more branching of CdSe and CdTe nanocrystals than monofunctional phosphonic acids and suggested that the bifunctional molecules may be important because they yield higher local acid concentrations at the molecular level than the monofunctional equivilent.

**Nucleation and Growth Kinetics.** To gain more insight into the mechanisms controlling the influence of diamine concentration on the equilibrium branch morphology, we have studied the kinetics of branch growth for different concentrations of DAP, with particular emphasis on the nucleation event and early growth stages. For 80 mM DAP, the induction time for branch nucleation on the columnar facets is 30 min, while growth on the (0001) surface begins essentially immediately (Figure 4). After 10 min of incubation (Figure 4a), significant growth is already observed on the basal plane, in the form of a dense array of nanorods on the order of a few nanometers in width oriented along ⟨0001⟩. No change is observed on the $\{10\bar{1}0\}$ facets of the primary ZnO rod (Figure 4b) until a nucleation burst at 30 min forms polycrystalline regions on the primary ZnO crystal (Figure 4c−e). At 40 min, the first nascent oriented crystals are seen to emerge from a dense polycrystalline coating that now covers the primary ZnO crystal (Figure 4f). At 50 min (Figure 4g), many of these emerging crystals are observed and are clearly aligned in the preferred orientation of ∼80° to the *c*-axis of the primary crystal. After 1 h, the aligned crystals have grown larger and cover the $\{10\bar{1}0\}$ facets of the crystal, while the dense growth on the basal plane has continued uniformly. After 3 h of incubation, the aligned branches have coalesced into fewer larger branches, and the crystal growth on the (0001) has also coalesced to form an extension of the primary crystal along the *c*-axis. The ZnO branches continue to grow longer until 6 h of incubation, at which point they do not change with increasing incubation time.

The kinetics of the branch crystal nucleation and growth are sensitive to diamine concentration, but the process is very similar. When the DAP concentration is reduced approximately in half (43 mM), nucleation occurs essentially instantaneously upon incubation (Figure 5a). After 10 min of incubation, the primary ZnO crystal is already covered by the polycrystalline layer, and nascent aligned branches have begun to grow. After 20 min (Figure 5b−c), the ZnO structure is at a similar state as the crystal at 50 min with 80 mM DAP (cf. Figure 4g), with many nascent aligned branches on the prismatic facets and about 200 nm of dense crystal growth on the basal plane. Figure 5c shows clearly that the nascent branches are aligned in the same twin configuration (80° angle) observed for branches at steady state. As with the higher DAP concentration, the aligned crystals continue to grow larger and ultimately cover each prismatic facet (Figure 5e). However, at the lower DAP concentration, the number density of aligned crystals is always higher, and the growth stops at an earlier stage with less coalescence of the smaller branches into larger branches (Figure 5f). At a higher DAP concentration (125 mM), growth on the basal plane of the primary crystal occurs rapidly (Figure 5g) as with the other concentrations, but nucleation of branches on the $\{10\bar{1}0\}$ facets is not observed until 4 h of incubation (Figure 5h). The kinetics of the growth on the basal plane at 125 mM DAP is approximately the same as that for 80 mM DAP and probably occurs prior to growth on the prismatic facets because the surface energy is higher on this surface. As with all growth with diamines (except at low concentrations of EDA), the basal plane of the primary crystal grows tapering into a point (see transition from Figure 5g to 5h to 5i, and additional images in Figure S5). After 10 h of incubation in 125 mM DAP, the branch crystals still continue to grow larger (Figure 5i). Nucleation of new crystals continues during the 10 h window of growth as evidenced by the increasing branch size distribution with longer

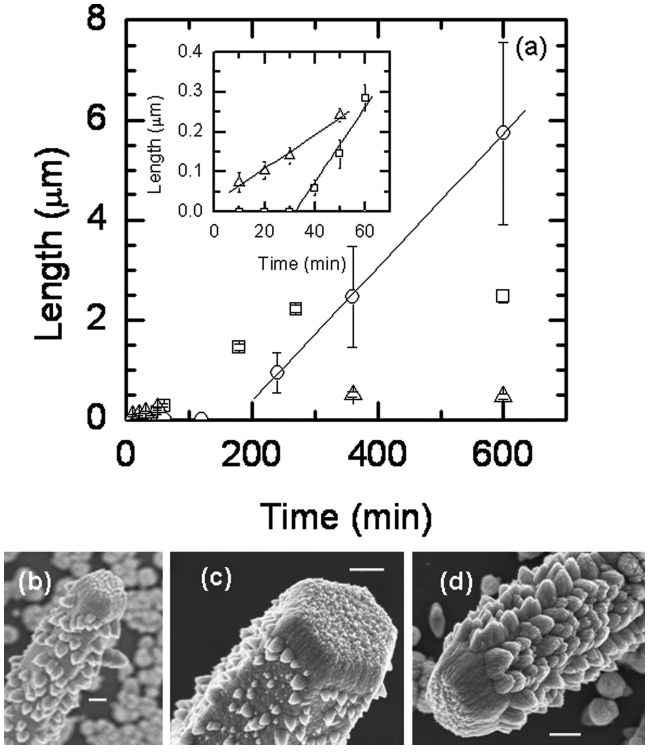


***Figure 6.*** Nucleation and growth kinetics for DAP concentrations of 43 mM, △; 80 mM, □; 125 mM, ○. (a) Branch crystal length vs time (inset shows magnified view of lower left corner of plot). Average growth rate (slope of linear fit to mean length in linear growth range) for 43, 80, and 125 mM is 4.3, 9.4, and 13.4 nm/min, respectively. Branch lengths are measured in same manner as that for Figure 2 measurements. SEM images in (b−d) show similarity between higher DAP concentration at early time and lower DAP concentration at equilibrium: (b) 30 mM DAP at 8 h, (c) 80 mM DAP at 50 min, (d) 80 mM DAP at 60 min. The branch growth for 30 mM DAP is terminated when the growth process is somewhere in between the 50 and 60 min stage for 80 mM DAP. Scale bars are 500 nm. The data points and error bars are as those for Figure 2. An image of multiple crystals in (b) is provided in the Supporting Information; Figure S6 and the images are compared at the same scale in Figure S10.

incubation times; note the smaller branches observed at 4 and 10 h (Figure 5h,i), including some small tertiary branches growing on the large secondary branches after 10 h of growth (Figure 5i).

**Mechanisms Controlling Secondary Crystal Morphology and Size.** Much of the observed morphology variation with diamine concentration is explained by the nucleation and growth kinetics. Figure 6 summarizes and quantifies a comparison of the kinetics for the three different DAP concentrations. After nucleation, the length of the branches increases linearly with time until the reactants begin to be depleted in the bulk solution phase and then branch growth is suspended (panel a). After 1 h of incubation, branch growth is in the linear range for 43 mM and 80 mM DAP (inset panel a), while nucleation has not yet occurred for 125 mM DAP. Extrapolation of a linear fit to the 43 mM data shows that nucleation is essentially instantaneous, and a linear fit to each set of data in the linear region shows that while the induction time increases, the growth rate also increases, with increasing DAP concentration. In other words, at low diamine concentration, nucleation is fast and growth is slow, so many aligned branches have time to form before the first branches grow significantly. As diamine concentration is increased, faster branch growth and slower nucleation lead to fewer and larger branch crystals. Near the upper limit of the branch-growth concentration range (125 mM DAP), nucleation is so slow and growth is so fast that few branches form at the same time. Thus, the branches are polydisperse and sparsely populated so they do not coalesce (cf. error bars in Figure 6a, and images Figure 5h,i). Also, because of the slow, sparse nucleation, there is no confinement on the direction of growth of the branches formed with 125 mM DAP, so they sample both preferred orientations (80° and −80° to the *c*-axis)[1] evenly, resulting in less ordered secondary structures.

In addition to the effect of nucleation and growth kinetics, the diamine concentration plays another role in shaping the final morphology of the branch crystals at equilibrium. Increasing diamine concentration increases the solubility of $Zn^{2+}$, which reduces the amount of homogeneous precipitation.[41] Thus, at lower amine concentrations, there is more homogeneous precipitation, which causes faster depletion of the $Zn^{2+}$ in solution, thus suspending the growth process at an earlier stage with less coalescence of the branch crystals. This is clear from Figure 6b, which shows the equilibrium state of branches formed at 30 mM DAP. The morphology is similar to that observed for higher DAP concentrations at early growth times, prior to coalescence of the branches to cover the facets. The growth of the branches at 30 mM DAP is suspended at a stage somewhere in between that for 80 mM DAP at 50 and 60 min (Figure 6c and d) because, at the lower DAP concentration, homogeneous precipitation depletes the supply of $Zn^{2+}$ earlier in the branch development process. Also note that as the diamine concentration is increased, the overall size of the secondary ZnO crystals (including all branches) increases even while the solubility increases, which also indicates the promotion of heterogeneous over homogeneous growth.

Perhaps the most interesting phenomenon in secondary branch growth is the transition from randomly oriented nuclei to branches aligned in a preferred orientation. Our observation of the early growth kinetics suggests a mechanism for this that is analogous to Ostwald ripening, whereby the nuclei with the most energetically favorable orientation grow at the expense of the misaligned crystals, which dissolve and recrystallize by epitaxial growth on the oriented crystals. This process is driven to minimize the interfacial energy between the new crystals and the primay ZnO crystal, which lowers the overall energy of the system after the nucleation burst. This is consistent with the observation of discrete oriented branches emerging sparsely out of the polycrystalline film coating the primary ZnO crystal (cf. Figures 4f,g and 5b,c). This is similar to the mechanism reported by Fang et al.[33] for the growth of ZnO flowerlike nanostructures from an initially polycrystalline cluster.

**Role of Diamine in Controlling Nucleation and Growth Kinetics.** In the previous section, the secondary crystal morphology was explained in part by the observed nucleation and growth kinetics as a function of diamine concentration, but the mechanism by which the diamine molecule controls the kinetics was not discussed. The effect of the amines on the solubility of $Zn^{2+}$ explains the observed nucleation kinetics. The free energy of nucleation $\Delta G$ for a nucleus of size $n$ is given by[56]

$$\Delta G = -nkT\ln(S) + (\sigma_n A_n - \sigma_i A_i) \qquad (1)$$

(56) Nielsen, A. E. *Kinetics of Precipitation*; Pergamon Press: New York, 1964.

where $kT$ is the Boltzmann temperature, $S$ is the degree of supersaturation, $A_n$ and $\sigma_n$ are the nucleus interfacial area and energy, respectively, and $A_i$ and $\sigma_i$ are the interfacial area and energy, respectively, of the interface replaced by the nucleus. Thus nucleation occurs when the free energy reduction of relieving the supersaturation exceeds the increase in the interfacial energy from nucleation. From this expression, classical nucleation theory predicts that the induction time $t_{ind}$ decreases with increasing supersaturation, viz.[56]

$$\log(t_{ind}) = C_1 + C_2\left(\frac{\sigma^3}{\log(S)^2}\right) \quad (2)$$

where $C_1$ and $C_2$ are constants for a fixed material system and temperature. The induction time is approximately 1, 30, and 240 min for DAP concentrations of 43, 80, and 125 mM, respectively. As the concentration of diamine increases, the degree of supersaturation of Zn decreases, which increases the induction time in agreement with classical nucleation theory and previous observations of thin film deposition kinetics.[57] The classical nucleation theory, however, does not account for the observed threshold concentration of diamine required to induce nucleation of branches. The lack of branch nucleation below the threshold diamine concentration does not imply $\Delta G > 0$ because nucleation and growth of ZnO still occurs but not in the form of branches; the existing ZnO surfaces of the primary crystal can support relief of the supersaturation without overcoming the free energy barrier of forming a new interface (eq 1 with the interfacial terms negligible); i.e., nucleation of the primary crystals already occurred in the primary growth stage. Something else, such as etching and/or adsorption, must change the interface of the primary ZnO crystal and promote nucleation over epitaxial growth.

The initial zero-order growth of the ZnO branches is consistent with previous observations of inorganic film deposition kinetics, such as FeOOH growth on self-assembled monolayers.[57] In that study, FeOOH films were grown in acidic aqueous solutions, and although increasing the acid concentration increased the solubility of $Fe^{3+}$, it did not affect the zero-order growth rate significantly. This is in contrast to the ZnO branch growth rate, which increases significantly with increasing base concentration and solubililty of $Zn^{2+}$. It is not clear why increased diamine concentration increases the growth rate.

**Model of Secondary Nucleation and Growth of ZnO.** The diamine-mediated secondary ZnO nucleation and growth model is summarized in Scheme 1. The effects of diamine concentration are summarized in panel a. As diamine concentration is increased from zero, it has no effect on crystal structure until a threshold concentration is reached, at which point nucleation is observed. As diamine concentration is increased above this critical nucleation concentration (CNC), the induction time increases, but the branches grow faster and growth is sustained longer because of the effect of increased Zn−amino complexes. Ultimately the concentration of diamine reaches an upper threshold where the solubility of $Zn^{2+}$ is increased such that no precipitation occurs. Further increase in diamine concentration beyond this saturation point results in dissolution of the primary ZnO crystals due to undersaturation of $Zn^{2+}$.

***Scheme 1***. Schematic Illustration of Nucleation and Growth Mechanism[a]

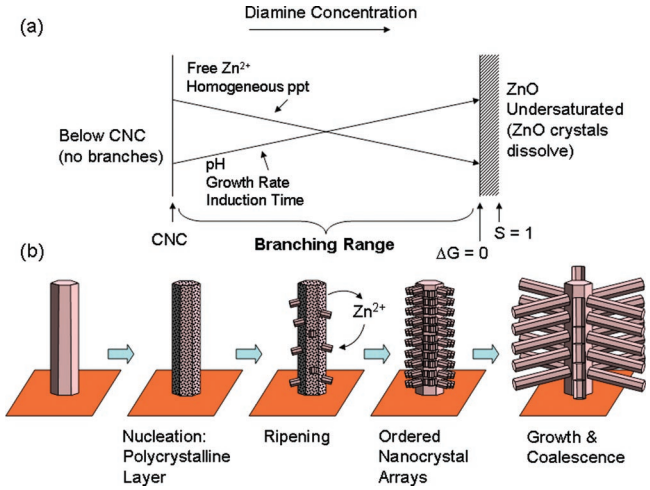


[a] (a) Diamine concentration zones and qualitative growth behavior. (b) Illustration of nucleation and growth process.

The branch nucleation and growth process is illustrated in panel b: *Step 1* - When the diamine CNC is reached, light surface etching induces nucleation of a polycrystalline layer by increasing the surface energy and creating nucleation sites. Other factors might also contribute to nucleation, such as adsorption of the diamines on the ZnO crystal. *Step 2* - Nuclei that are aligned in the most energetically favorable orientation (~80°) grow at the expense of the misaligned nuclei. This is energetically favored because it reduces the interfacial stress at the primary ZnO surface. *Step 3* - The misaligned nuclei are ultimately eliminated in favor of the oriented branches, which continue to grow larger at a higher rate along the *c*-axis, as typically observed for ZnO crystal growth because the (0001) planes have a higher energy. With sufficient concentration of diamine (which slows homogeneous precipitation, thus maintaining free $Zn^{2+}$ to continue growth), the aligned branch crystals coalesce and grow into larger single crystals. This is possible because they all have the same orientation. *Step 4* - Growth stops when Zn in solution is reduced below the solubility limit. This occurs at earlier stages of the general growth process as the diamine concentration is reduced because more Zn is lost to precipitation in the bulk.

## Conclusion

Secondary nucleation of ZnO branches on primary ZnO crystals is an unusual phenomenon regulated by diaminoalkane molecules in the secondary growth stage at concentrations approaching the Zn saturation point. The organic diamines control branch nucleation and growth through their effect on ZnO solubility through Zn−amino complex formation and pH. The secondary growth concentration range increases by a factor of 4 to 5 for each additional carbon in the diaminoalkane chain from EDA to DAP due to a concomitant increase in the solubility limit. Tunable growth is achieved with DAP and DAB but not with EDA. Extrapolation to longer chain lengths suggests that volume ratios on the order of 20% would be required for diaminopentane and the use of diaminohexane would probably not be possible because 100% diaminohexane would be required. DAP is the optimum molecule for controlling branch size because minimal concentrations are required and the melting

(57) Rieke, P. C.; Marsh, B. D.; Wood, L. L.; Tarasevich, B. J.; Liu, J.; Song, L.; Fryxell, G. E. *Langmuir* **1995**, *11*, 318−326.

point for DAB is 26 °C, which makes it difficult to manipulate at room temperature.

Observations of primary crystal surfaces imply that nucleation is induced on defect sites created by light surface etching. The induction time increases with diamine concentration, which is shown to be consistent with classical nucleation theory. The growth process is essentially identical at all diamine concentrations, but the final morphology of the secondary structures varies widely with diamine concentration from the effect of diamine on growth kinetics and competition with homogeneous nucleation, which depletes bulk $Zn^{2+}$ concentrations and suspends growth at an earlier stage in the branch development for lower diamine concentrations. Observations of the branch growth process suggest that a mechanism analogous to Ostwald ripening controls the transition from the polycrystalline film to the oriented branches. This mechanism may apply to other material systems, such as oriented $SnO_2$ branch growth on $\alpha$-$Fe_2O_3$ nanotubes,[37] which was reported to also begin with a polycrystalline coating nucleated in a secondary branch growth stage.

**Acknowledgment.** We thank Diana Moore and Alex Lee at Sandia National Laboratories for help with pH measurements and SEM samples, respectively, and Yingbing Jiang at the University of New Mexico for TEM images of the branch nuclei. This work was supported by the Sandia National Laboratories (SNL) Laboratory-Directed Research and Development Program (LDRD) and by the Division of Materials Sciences and Engineering, Office of Basic Energy Sciences, U.S. Department of Energy. SNL is a multiprogram laboratory operated by Sandia Corporation, a Lockheed Martin Company, for the Department of Energy under Contract DE-AC04-94AL85000.

**Supporting Information Available:** In the Figures 1, 4−6, single particles are shown, and the magnification of each image is adjusted to show clearly the branch morphology at each reaction condition. SEM images of multiple crystals for each reaction condition are provided in the Supporting Information to show that the individual crystals presented in the paper are representative. Also, SEM images of the crystals compared at the same magnification are provided for direct size comparisons. This material is available free of charge via the Internet at http://pubs.acs.org.

JA071209G